USGS
science for a changing world

Processing Strategy for Water-Gun Seismic Data from the Gulf of Mexico

U.S. Geological Survey Bulletin 2181

U.S. Department of the Interior
U.S. Geological Survey

Processing Strategy for Water-Gun Seismic Data from the Gulf of Mexico

By Myung W. Lee, Patrick E. Hart, *and* Warren F. Agena

U.S. Geological Survey Bulletin 2181

U.S. Department of the Interior
U.S. Geological Survey

U.S. Department of the Interior
Bruce Babbitt, Secretary

U.S. Geological Survey
Charles G. Groat, Director

Posted online December 2000, version 1.0
April 2001, version 1.1

This publication is available online at:
http://geology.cr.usgs.gov/pub/bulletins/2181/

Contents

Figures

Processing Strategy for Water-Gun Seismic Data from the Gulf of Mexico

By Myung W. Lee, Patrick E. Hart, *and* Warren F. Agena

Abstract

In order to study the regional distribution of gas hydrates and their potential relationship to a large-scale sea-floor failures, more than 1,300 km of near-vertical-incidence seismic profiles were acquired using a 15-in^3 water gun across the upper- and middle-continental slope in the Garden Banks and Green Canyon regions of the Gulf of Mexico. Because of the highly mixed phase water-gun signature, caused mainly by a precursor of the source arriving about 18 ms ahead of the main pulse, a conventional processing scheme based on the minimum phase assumption is not suitable for this data set. A conventional processing scheme suppresses the reverberations and compresses the main pulse, but the failure to suppress precursors results in complex interference between the precursors and primary reflections, thus obscuring true reflections.

To clearly image the subsurface without interference from the precursors, a wavelet deconvolution based on the mixed-phase assumption using variable norm is attempted. This non-minimum-phase wavelet deconvolution compresses a long-wave-train water-gun signature into a simple zero-phase wavelet. A second-zero-crossing predictive deconvolution followed by a wavelet deconvolution suppressed variable ghost arrivals attributed to the variable depths of receivers. The processing strategy of using wavelet deconvolution followed by a second-zero-crossing deconvolution resulted in a sharp and simple wavelet and a better definition of the polarity of reflections. Also, the application of dip moveout correction enhanced lateral resolution of reflections and substantially suppressed coherent noise.

Introduction

Gas hydrates are ice-like crystalline solids composed of water molecules surrounding individual gas molecules. Methane hydrates have been the focus of many investigations because of their natural abundance in the world's oceans and in permafrost regions (Kvenvolden, 1993). Gas hydrates may play an important role as a negative feedback control on global temperature fluctuations (Dillon and others, 1991; Paul and others, 1991), as a potential energy resource, and as a significant factor in sea-floor stability and safety issues (Dillon and others, 1993).

As part of an investigation of the potential relationship between gas hydrates and large-scale sea-floor failures in the Gulf of Mexico, more than 1,300 km of near-vertical profiles were acquired using three seismic sources: a 15-in^3 water gun, a deep-tow Huntec boomer, and Datasonics chirp system (Cooper, Hart, and Twichell, 1999). This study investigates the processing strategy for water-gun data in order to (1) maximize the advantage of the water gun, namely the high-frequency content of the source (as much as 1,000 Hz), and (2) minimize the disadvantage of the water gun, namely precursors to the main energy pulse.

The U.S. Geological Survey (USGS) was previously involved in the processing of seismic data acquired in Eniwetok Atoll, Marshall Islands, using both 15-in^3 and 80-in^3 water guns (Grow and others, 1986). One purpose of that survey was to clearly image the boundaries of craters created by nuclear bomb testing in the 1950's. Resulting images from the conventional processing using a spiking deconvolution indicated that the image of the crater was obscured by the interference of precursors from the water gun. After applying a wavelet deconvolution using the variable norm deconvolution method (Gray, 1979), the seismically transparent sediments between the crater floor and 80 m in depth, representing transient crater-fill beneath the inner bathymetric crater, were clearly imaged (Grow and others, 1986).

Also in 1996, the U.S. Geological Survey together with the National Geographic Society acquired a single-channel seismic data set in the Chesapeake Bay area, near Norfolk, Va., using a 15-in^3 water gun and a generator injector gun. The purpose of this study was to accurately map an impact structure by resolving the basement surface, the basement structure, internal disruptions in stratigraphy, and possible faulting (Poag and others, 1999; D.R. Hutchinson, written commun., 1996). The processing of this data set was more complicated than that of the Eniwetok data set because only a single channel was acquired and the water depth was much shallower. The direct arrivals and reflections were intermixed, and it was difficult to extract an accurate water-gun source wavelet as mentioned in Lee (1999). However, even though the wavelet extraction was not optimum, processing with wavelet deconvolution provided

a much-improved seismic section compared to one obtained by using conventional methods, i.e., using a spiking or predictive deconvolution (Lee, 1999).

In our study area (Gulf of Mexico), the shallow stratigraphy and structure are complex, largely due to salt tectonism, and the survey area is further characterized by a complex basin-and-ridge morphology. The sedimentary section is highly faulted, and hydrates commonly occur within local mound-like deposits and near buried salt diapirs and faults (Cooper, Hart, and Twichell, 1999). The precursors of the water-gun seismic source interfere with the primary reflections and make interpretation of stratigraphy in areas of complex geology troublesome and difficult.

This paper describes the details of the processing strategy used to attack a problem generally inherent in seismic data acquired with a water gun, i.e., a source wavelet problem similar to the problem encountered in the Eniwetok Atoll study. Therefore, the main focus of this investigation is on wavelet extraction and deconvolution.

Acknowledgments

We thank John Miller and Dave Taylor for their helpful comments and suggestions and Chris French for his art work on illustrations. William Dillon's encouragement throughout the investigation is also appreciated.

Data Acquisition

During April 1999, the U.S. Geological Survey conducted a seismic survey in the Garden Banks and Green Canyon regions of the Gulf of Mexico (fig. 1) with the R/V Gyre, owned by Texas A&M University. The general objectives were to acquire very high resolution seismic-reflection data and side-scan sonar images of the upper and middle continental slope (in water 100–1,200 m deep) to study the acoustic character, distribution, and potential effects of gas hydrates within the shallow subsurface. During this cruise, water-gun multichannel seismic-reflection, chirp seismic-reflection, and side-scan sonar data were collected. The seismic sources included a 15-in^3 water gun, a deep-tow Huntec boomer, and a deep-tow Datasonics chirp system. Relevant information on water-gun multichannel seismic-reflection data is discussed here, and detailed survey information for all of the data sets is found in the cruise report by Cooper, Twichell, and Hart (1999).

Navigation was done using the USGS real-time YONAV system, which provided gun-shot-triggers on a constant-time basis. Water-gun multichannel seismic data were recorded using a 24-channel ITI streamer with 10-m group interval and three phones per group. The farthest offset channel was about 270 m behind the source. The streamer was towed at an estimated depth of 1–3 m (there were no depth sensors on the streamer), and a 15-in^3 water gun, towed about 1-m depth, was fired at 6-second intervals.

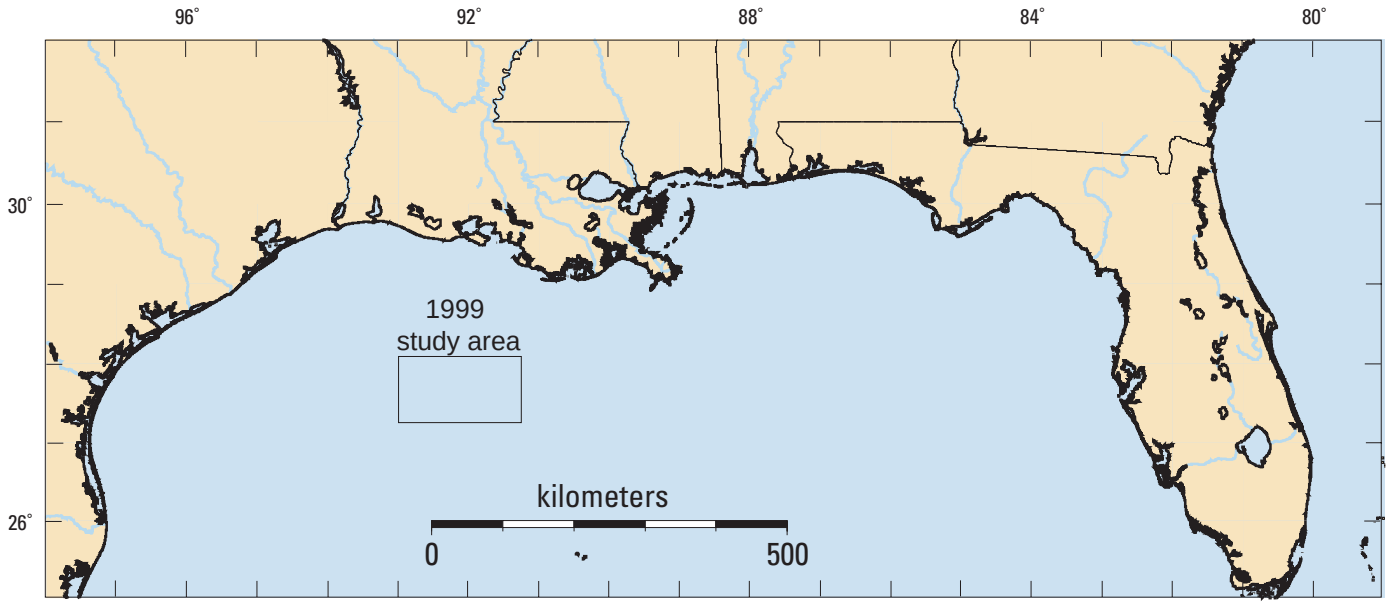

Figure 1. Location map of the seismic survey.

On the cruise, wind conditions were highly variable and seas were mixed (generally less than 4–6 ft). Data quality is generally good but is affected in various places by noises such as cross-talk between boomer and water-gun seismic reflection systems, other seismic-shooting ships, and nearby drilling operations.

Data Processing

The processing flow for the data set is given in the following 10 steps:

1. Geometry definition
2. Wavelet deconvolution
3. Second-zero-crossing predictive deconvolution
4. True amplitude adjustment
5. Velocity analysis
6. Common-offset-domain dip moveout correction
7. Normal moveout correction with DMO velocity
8. 12-fold stack
9. Migration
10. Band-pass filtering, mute, phase reverse, and plot.

The shot interval was based on time (6 seconds) and, due to the speed of the vessel, varied between 10 and 13 m. To have a uniform common-mid-point (CMP) interval for the geometry, a 10-m shot interval was assumed and the data were sorted into 12-fold CMP gathers.

Relative true amplitudes were recovered by applying a power law (T^2) up to 2 seconds, and variation of source strength and receiver coupling were compensated for by applying surface-consistent amplitude corrections. This amplitude correction computes amplitudes in a given time window and decomposes them into source, receiver, channel, and offset components using an iterative method. Based on the decomposed amplitude component, a scalar is calculated and applied to each trace in order to preserve relative true amplitude.

Velocity analysis was problematic because of the offset distance. As a rule of thumb, the maximum target depth of data is in the range of the maximum offset. The maximum offset for these data was 270 m, so the optimum target depth is about 300 m, which is much shallower that the target depths of this study. The maximum arrival-time difference between near and far traces for a reflector at a depth of 500 m is 15 ms when the root-mean-square (RMS) velocity is 1.5 km/s. This arrival-time difference decreases as the velocity increases, and it is 12 ms if the RMS velocity is 2 km/s. There is only a 3 ms time difference between two moveout times in differentiating a RMS velocity of 1.5 km/s from 2 km/s. Therefore, it is difficult to accurately determine velocities. However, stacking-velocity analysis is not a severe problem because stacking-velocity analysis is based only on the stack power and can have a large error and still provide a good-quality stacked section. However, using such stacking velocities for migration could be problematic in addition to the fact that the trace-to-trace distance is not really uniform because the shot interval varied.

Wavelet Deconvolution

It is well known that a water gun produces a mixed-phase wavelet and that it is difficult to extract the wavelet based on the minimum phase assumption used with spiking deconvolution. In order to deconvolve a mixed-phase wavelet, Wiggins (1977) developed the maximum entropy deconvolution (MED) method. The extension of the MED method, which is called variable norm deconvolution (VND), was investigated by Gray (1979). In this paper, VND is employed to extract a water-gun signature and to perform wavelet deconvolution. Previously, it was concluded that VND provided optimum results for the water-gun data acquired in Eniwetok Atoll (Grow and others, 1986).

The variable norm (U) for the Wiggins-type algorithm is defined as:

$$U(x,\alpha,2) = \log \prod_{j=1}^{m} \frac{\left[\frac{1}{n}\sum_{i=1}^{n}\left|x_{ij}\right|^{\alpha}\right]^{n/\alpha}}{\left[\frac{1}{n}\sum_{i=1}^{n}\left|x_{ij}\right|^{2}\right]^{n/2}} \qquad (1)$$

where

X_{ij} is the i-th sample of the signal recorded on channel j,

n is the sample number per channel,

and α is a constant greater than 2.

The essence of VND is to iteratively estimate an inverse filter such that U(x,α,2) shown in equation 1 is maximized. When $\alpha = 4$, this is MED by Wiggins (1977).

Figure 2 shows extracted water-gun wavelets with $\alpha = 2.2$ for lines 20 and 21. These wavelets were extracted from shots 100 to 110 for both lines. Notice the low-frequency precursors for both wavelets. The precursor precedes the main pulses by about 18 ms. The details of the extracted wavelet are different from each other even though the same gun was used. The source signatures vary along the seismic line, partly because the short-period source or receiver ghosts change as the streamer fluctuates and the sea conditions change. However, we assume that the typical source signature in each line is constant. Thus, a representative wavelet is extracted from each line separately and an inverse filter (deconvolution filter) is designed based on the extracted wavelet and applied to the corresponding lines.

The result of wavelet deconvolution for line 20 is shown in figure 3. Two shot gathers on the left are original records, and the right two shot gathers are corresponding records after wavelet deconvolution based on the wavelet shown in figure 2. In the deconvolved gathers, the problematic precursors are gone and the main pulse is almost a zero-phase wavelet. The waveforms for the near traces look like a minimum-phase wavelet (trough-peak combination), and this could be caused by interference of the ghosts. This will be addressed in the following section. However, the waveform at the far trace of each gather is close to a zero-phase wavelet.

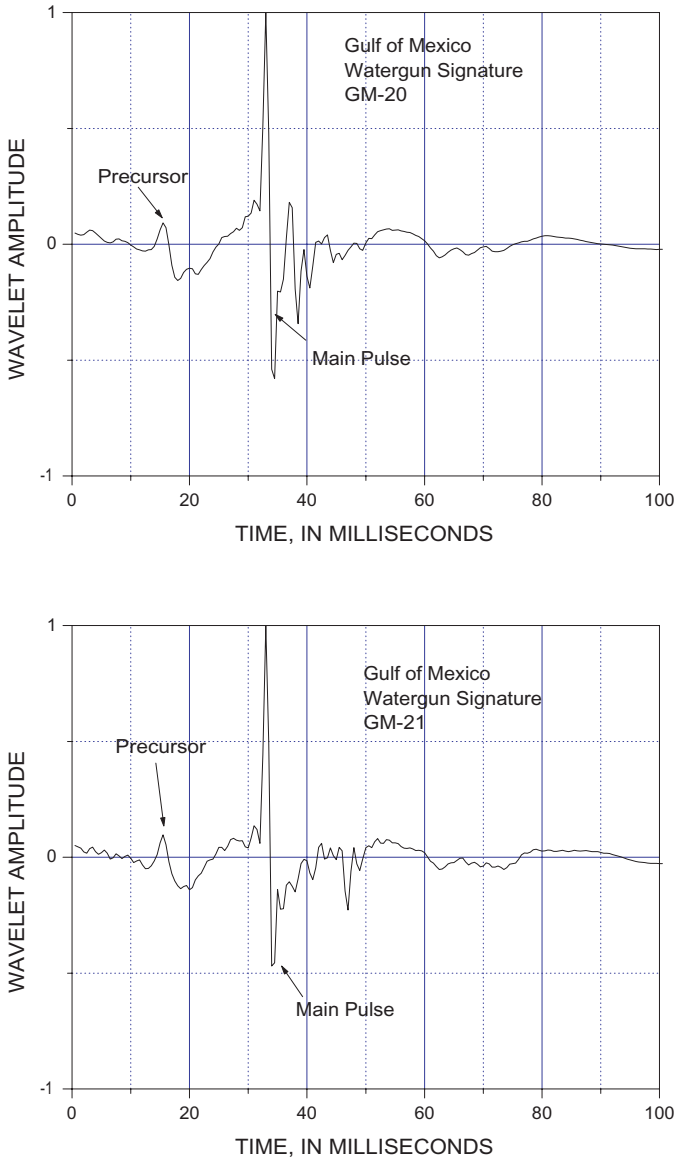

Figure 2. Extracted water-gun wavelets using the variable norm deconvolution method by Gray (1976). Note the similarity between two extracted signatures and precursors about 18 ms ahead of the main pulses.

Ghosting Effects and Second-Zero-Crossing Deconvolution

Original shot records and wavelet deconvolved records, shown in figure 3, clearly indicate that there are two first arrivals—two precursors and main pulses between 240 ms and 280 ms. The time difference between these two arrivals becomes larger as the offset increases and is about 10 ms at the far trace. The details of the first arrival after wavelet deconvolution can be seen in figure 4. Notice that the amplitude of the second arrival is almost as big as the first arrival and its phase is opposite of the first arrival. These waveform and amplitude characteristics suggest that the second arrival is a ghost.

In the case where source and receiver depths are constants, the arrival-time difference between the primary reflection and source/receiver ghost decreases but the observed time difference between primary and ghost arrivals increases as the offset increases. In order to explain the observed time difference between two arrivals, arrival times of primary and ghosts were calculated with the equation shown in the Appendix. One possible model is created by assuming that the streamer (receiver) was sinking linearly with increasing offset at a rate of 0.5 m per channel. The arrival times of the primary and the receiver ghost are shown in figure 5. Note that arrival times from this simple model agree well with those shown in figure 4. These ghosts interfere with the primary reflections and should be suppressed.

As shown previously, the moveout times of the primary reflections and their ghosts are markedly different. Therefore, to produce a clear image, the ghosting effect should be minimized. Since the wavelet deconvolution was already performed and the wavelet is almost zero-phase, a second-zero-crossing deconvolution is applied to the data to minimize the ghosting effect. Second-zero-crossing deconvolution is a type of predictive deconvolution where the prediction distance is the second zero crossing of the auto-correlation of the trace. A single window with a 20-ms operator length was used. The result after application of a second-zero-crossing deconvolution is a shown on the right of figure 4; it can be seen that the amplitudes of the ghost reflections are markedly reduced.

Dip Moveout Correction

The stacking velocity or NMO velocity depends on the dip of the reflector. It is well known that the conventional stacking method cannot stack both a flat and dipping layer occurring at the same time because of the dip dependence of the stacking velocity. The dip moveout (DMO) process is a method used to improve the stack quality by compensating for the dip effect in the NMO equation. DMO correction transforms nonzero-offset seismic data in a CMP gather into to the same zero-offset reflection times and reflection points for all offsets. This transformation improves velocity estimates, provides higher lateral resolution, and attenuates coherent noise (Deregowski and Rocca, 1981; Deregowski, 1986; Yilmaz, 1987).

DMO corrections can be applied in the common-offset domain or in the shot domain. Tests indicated that shot-domain DMO did not work well with this data set, partly because shot-domain DMO is more sensitive to the errors in the NMO velocity and degrades high frequencies at steep dips. Also, the 24-fold with a maximum offset of 270 m is not particularly suitable for the shot-domain DMO. However, common-offset-domain DMO indicated that, even though DMO did not improve velocity analysis due to the short offset distance, DMO processing suppressed coherent noise and improved lateral resolution significantly.

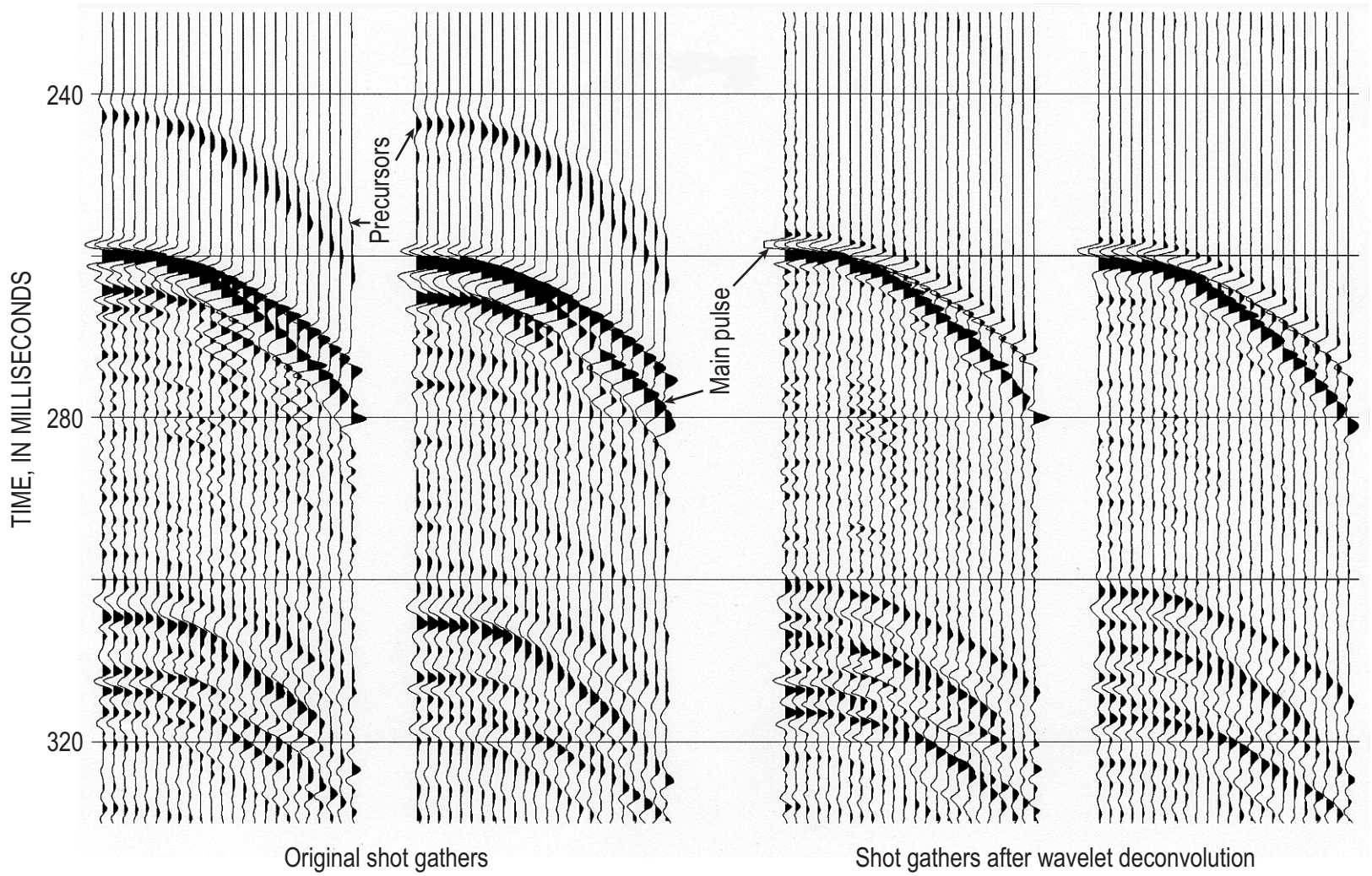

Figure 3. Unprocessed shot gathers (left two panels) and the same gathers after applying wavelet deconvolution (right two panels) for line 20.

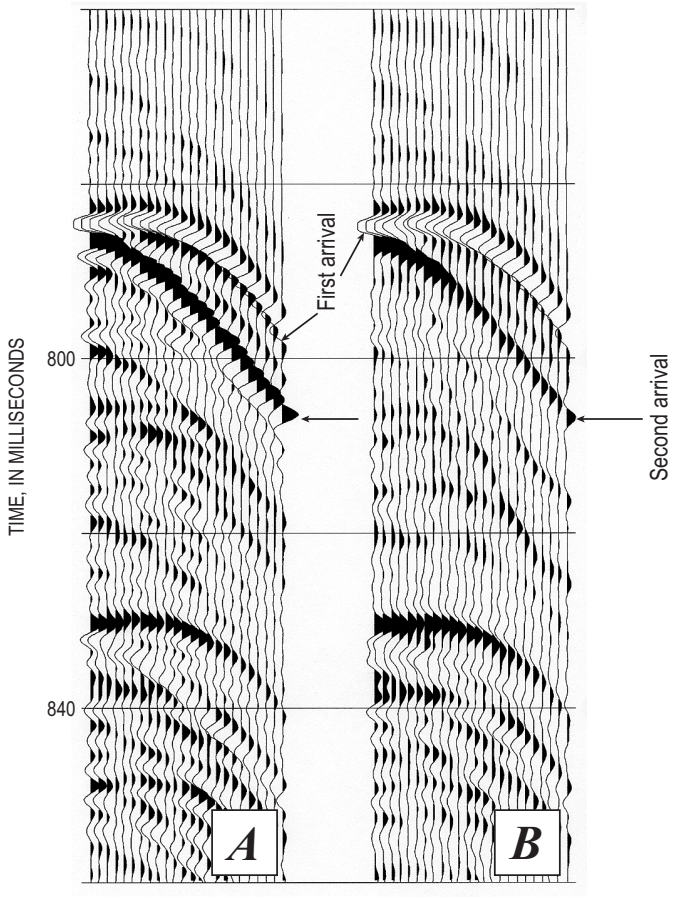

Figure 4. Plot showing a shot gather. *A*, After wavelet deconvolution. *B*, After wavelet deconvolution followed by second-zero-crossing predictive deconvolution.

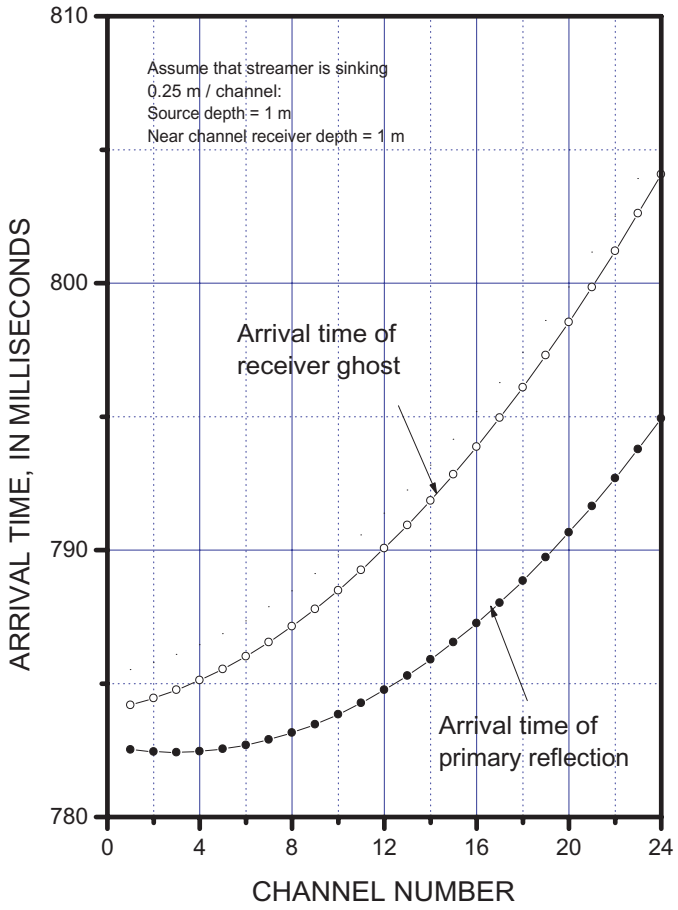

Figure 5. Graph showing arrival times of primary reflections and corresponding ghost reflections. Parameters are: number of channels = 24, offset of near channel = 30 m, group interval = 10 m, water depth = 588 m, source depth = 1 m, receiver depth at near channel = 1 m, and receiver depth at far channel = 7 m. It is assumed that the streamer is linearly sinking at a rate of 0.25 m/channel.

Discussion

The effect of the various processing techniques presented can be assessed from the stacked sections shown in figure 6. Figure 6*A* shows the stacked section without any deconvolution. The processing sequence for figure 6*A* is geometry definition, automatic gain control (AGC) with 100-ms window, normal moveout (NMO) correction, 12-fold stack, phase reversal (180° phase shift to make the water-bottom reflection peak) and band-pass filtering (40–600 Hz). Notice the stacked precursor, arriving about 18 ms before the main water-bottom reflection. Also notice stacked precursors around 590 ms, which are precursors of the reflection around 610 ms. These low-frequency precursors are persistent throughout the section and interfere with primary reflections.

Figure 6*B* shows the result of applying wavelet deconvolution. The processing sequence is identical to those for figure 6*A* except that wavelet deconvolution is applied before AGC. Notice that the precursors are greatly reduced throughout the section and waveforms are much sharper. Also, the reflections near 800 ms are well imaged in figure 6*B* but are obscure in figure 6*A*. The quality of figure 6*B* is significantly better than that of figure 6*A*, but the ghosting effects mentioned earlier are till evident, particularly for the water-bottom reflections.

Figure 6*C* shows the result of applying wavelet deconvolution in tandem with a second-zero-crossing deconvolution. The effects of ghosting are suppressed in figure 6*C*, and the waveform of the reflections is clean and sharp.

A typical and conventional processing strategy for the water-gun data is applying a minimum-phase spiking deconvo-

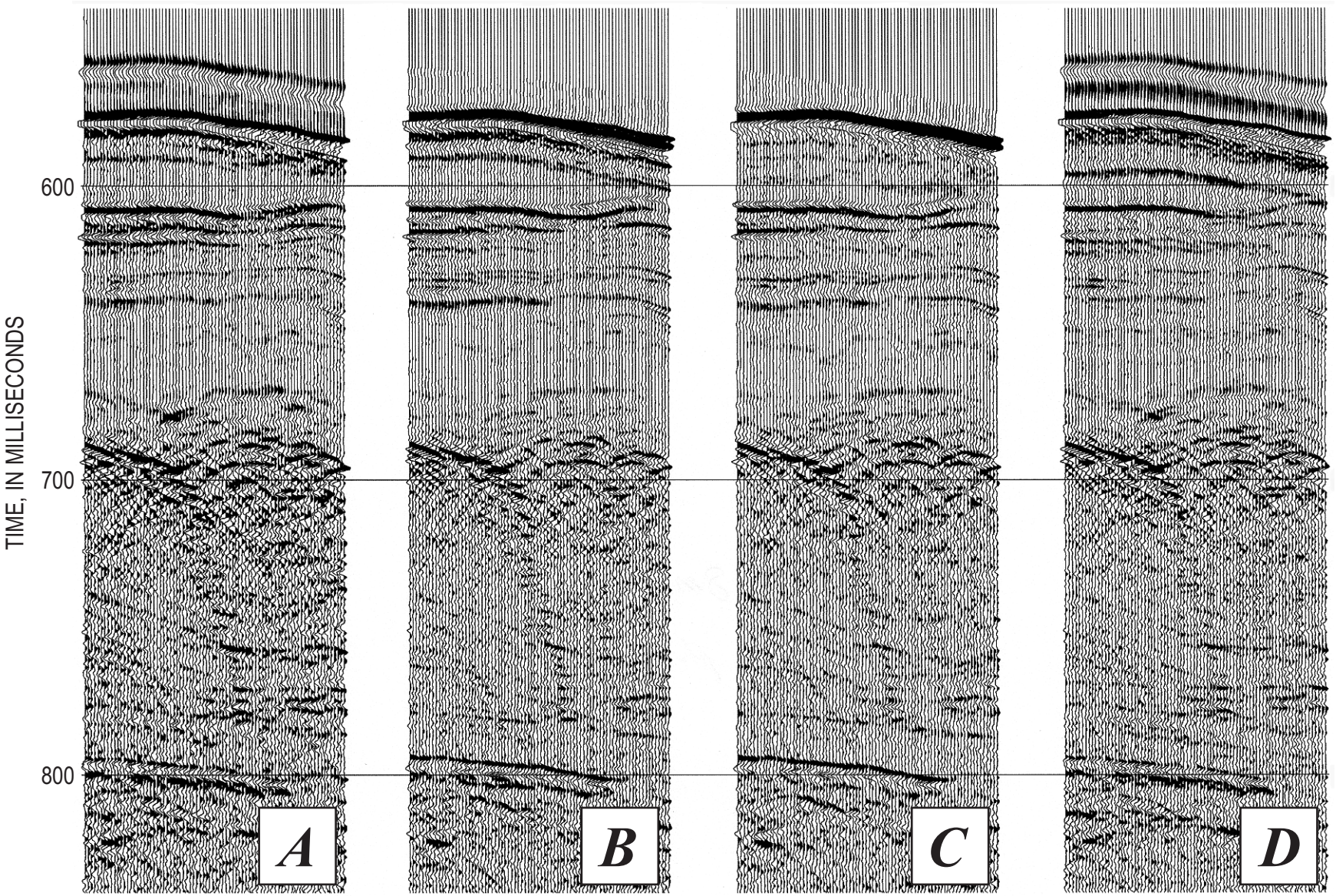

Figure 6. Result of different processing flows. General processing flow includes geometry definition (5-m CMP interval), AGC with 100-ms window, NMO, and stack. Precursors were not muted for figures 6*A* and 6*D* to emphasize the precursor problem of the water gun. *A*, Section with general processing flow mentioned above. *B*, Section with processing flow identical to figure 6*A* except that wavelet deconvolution was applied before AGC. *C*, Section with processing flow identical to figure 6*B* except that a second-zero-crossing predictive deconvolution was applied after wavelet deconvolution. *D*, Section with processing flow identical to figure 6*A* except that a spiking deconvolution was applied before AGC.

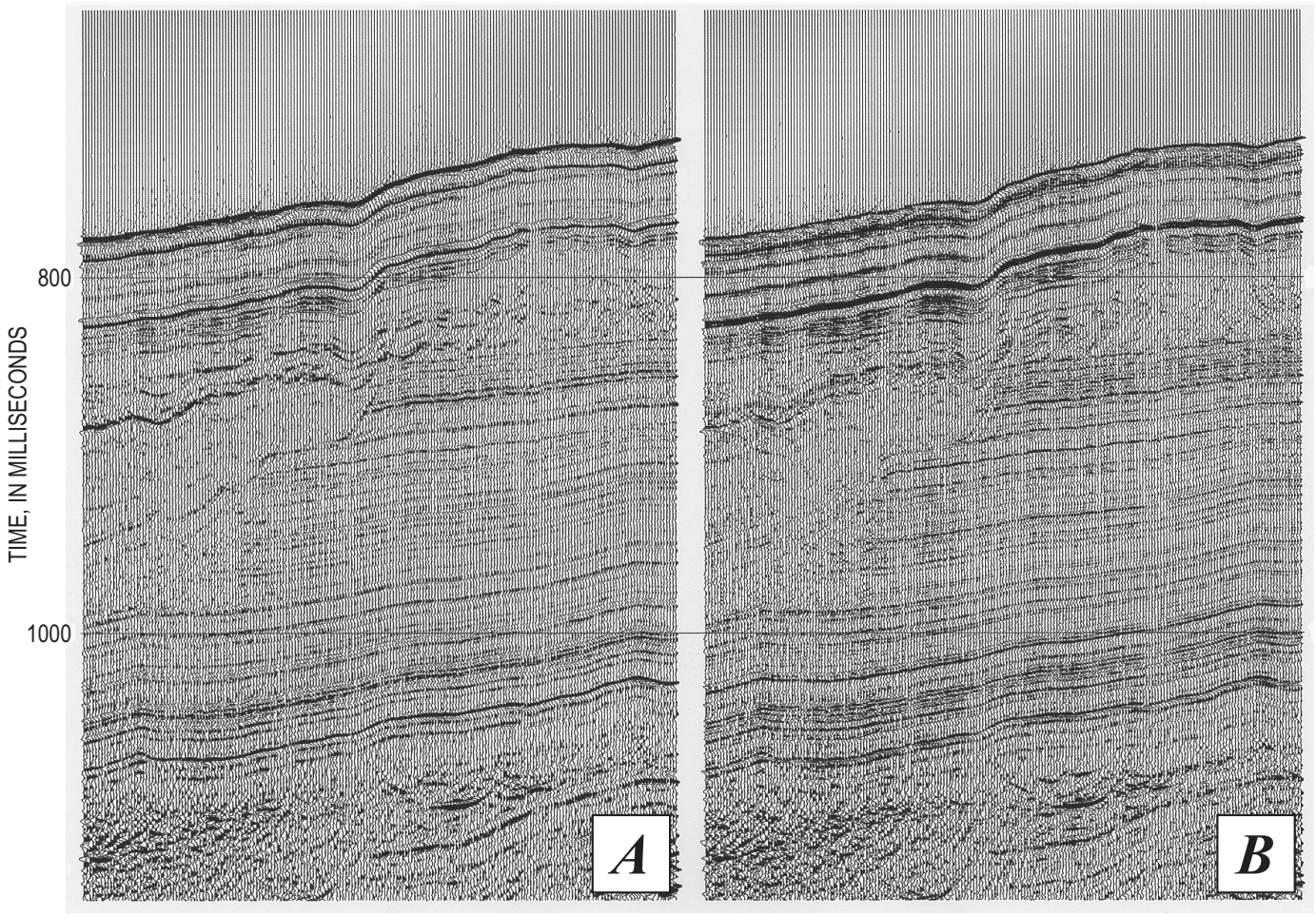

Figure 7. Portion of the migrated RTA section of line 21 for comparison between the two processing strategies. Frequency range is 40–600 Hz. *A*, Processing strategy with a wavelet deconvolution followed by a second-zero-crossing predictive deconvolution. This is the processing strategy adopted here for the processing of Gulf of Mexico data. *B*, Conventional processing strategy using a spiking deconvolution.

lution and muting the precursor of water-bottom reflections. Figure 6*D* shows the stacked section using a conventional method without mute. Because a spiking deconvolution not only collapses a source wavelet but also removes repetitive energy like ghosts or reverberations, the stack section shown in figure 6*D* shows a clean and sharp water-bottom reflection. However, because spiking deconvolution assumes a minimum-phase wavelet, the precursors are still present in the stacked section and the phase of the wavelet is obscure.

To assess the overall performance of the processing strategy adopted for the Gulf of Mexico data, a portion of the relative true amplitude (RTA) section for line 21 is shown in figure 7. The processing sequence of figure 7*A* is identical to that of figure 6*C* except that a programmed gain function and surface-consistent amplitude adjustment rather than AGC are applied and the data are migrated. The processing sequence of figure 7*B* is identical to that of figure 6*D* except that a programmed gain function and surface-consistent amplitude adjustment are applied and the data are migrated.

A cursory interpretation of figure 7*B* indicates that the wavelets are sharp and clean, and it looks like a good-quality seismic section. However, comparing figure 7*B* with figure 7*A*, we conclude that many of the primary reflections in figure 7*B* are interfered with by precursors (as demonstrated in fig. 6)

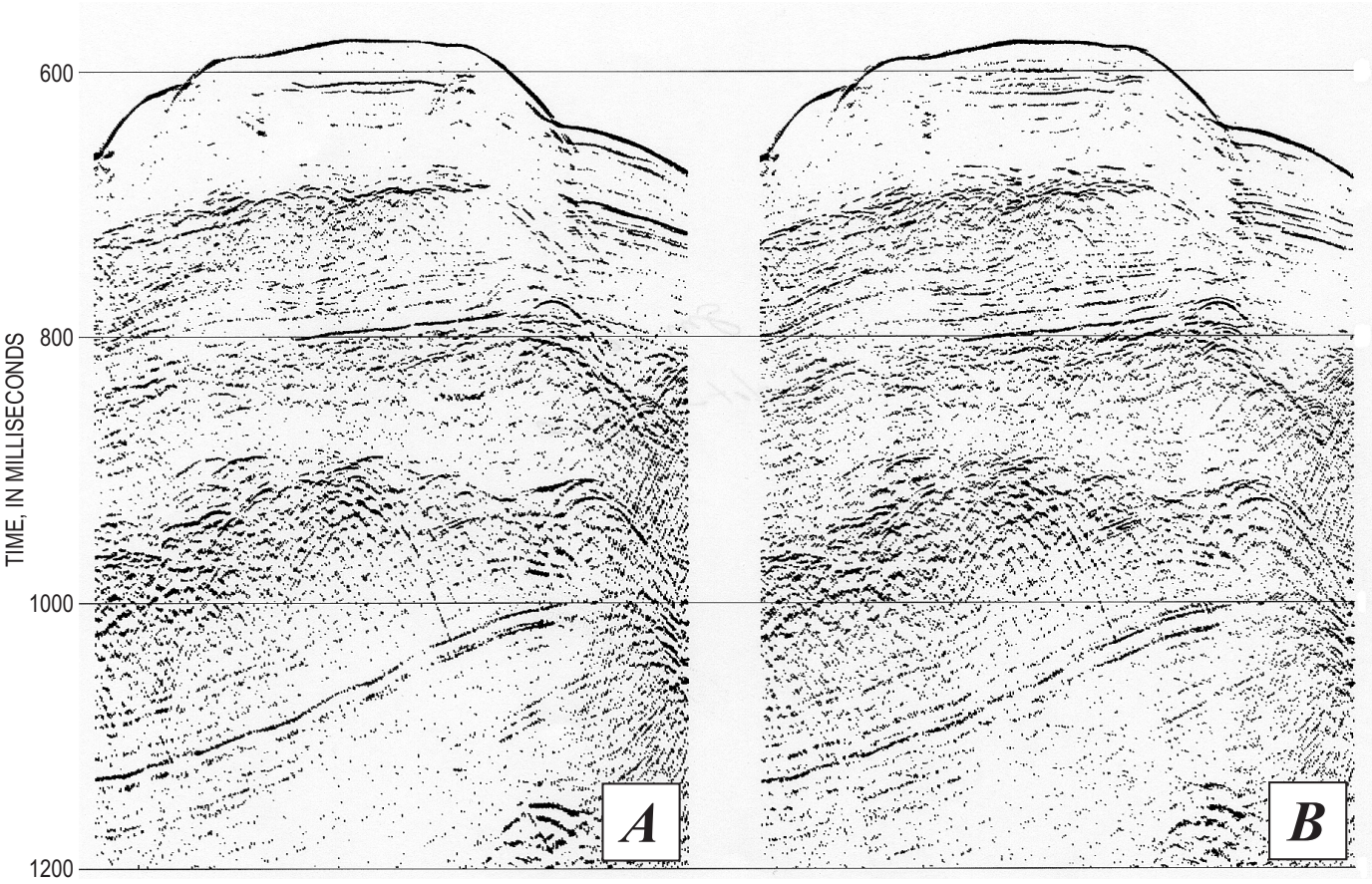

Figure 8. Portion of stacked RTA section of line 20 for comparison between the two processing strategies. Frequency range is 20–400 Hz. *A*, Processing strategy with a wavelet deconvolution followed by a second-zero-crossing predictive deconvolution. This processing strategy is adopted here for the processing of Gulf of Mexico data. *B*, Conventional processing strategy using a spiking deconvolution.

and the phase of wavelet is mixed. In other words, the stack quality of section 7*B* is inferior to that of figure 7*A*. This example illustrates that the wavelet deconvolution of water-gun data provides better quality processed data, particularly for use in stratigraphic interpretation. Another example is shown in figure 8: figure 8*A* shows the RTA stacked section processed using wavelet deconvolution, and figure 8*B* contains the RTA stacked section processed using spiking deconvolution. Figures 7 and 8 clearly demonstrate that the processing strategy, which includes wavelet and second-zero-crossing deconvolution instead of a spiking deconvolution seems to be optimum for this data set.

An example of DMO processing is shown in figure 9. The processing flow for figure 9*A* is identical to that of figure 7*A*, which is the migrated section without DMO processing. A migration velocity model for figure 9 was developed by reducing the stacking velocity values by 10 percent and smoothing them. Figure 9*B* shows the migrated section with common-offset-domain DMO application. Figure 9 indicates that, with the application of DMO, dipping reflections are imaged better and overall signal-to-noise ratio is much improved by reduction of coherent noise. The migrated section with the application of shot-domain DMO did not show any noticeable improvement over the migrated section without DMO. Because the maximum source-receiver offset is so short in this data set, DMO processing has its limitations, but, as indicated in this example, application of common-offset-domain DMO is still worthwhile for analysis and interpretation of areas of complex geology.

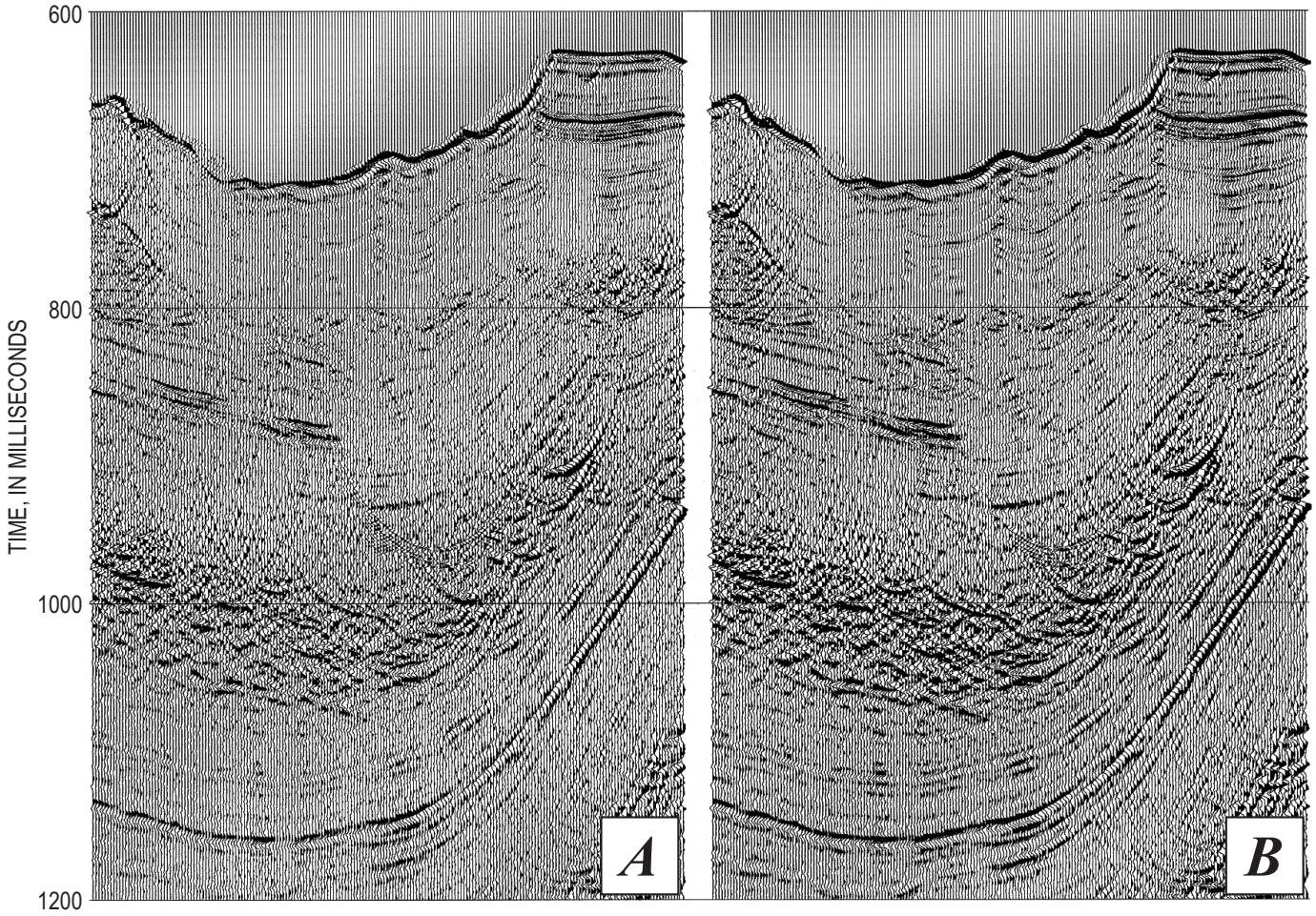

Figure 9. Portion of line 20 for comparison between the migrations with and without DMO. Frequency range is 20–400 Hz. *A*, Migrated section without DMO. *B*, Migrated section with DMO.

Conclusions

This study indicates that a processing strategy of wavelet deconvolution followed by a second-zero-crossing deconvolution is optimum for the processing of the Gulf of Mexico seismic data acquired with a water-gun source. The following conclusions can be drawn from the study:

1. The use of wavelet deconvolution is essential to collapse the water-gun signature as well as to remove the precursor. The highly mixed phase water-gun signatures are accurately extracted by using the variable norm deconvolution method.
2. Predictive deconvolution—such as a second-zero-crossing deconvolution applied after wavelet deconvolution—is important to further suppress ghosts and any other reverberations.
3. The dip moveout process, in the common-offset domain rather than in the shot domain, enhances lateral resolution and suppresses coherent noise, providing a much-improved migrated section.
4. Conventional processing including spiking deconvolution instead of wavelet deconvolution provides an apparently good quality seismic section, but close interpretation reveals that it contains numerous precursors that interfere with primary reflections. Care must be taken in interpreting the seismic stratigraphy on sections processed in this way.

References Cited

Cooper, A.K., Hart, P., and Twichell, D., 1999, High-resolution seismic-reflection survey of potential gas hydrate deposits beneath the upper continental slope of the northern Gulf of Mexico: San Francisco, Calif., AGU Annual Meeting, December 1999.

Cooper, A.K., Twichell, D., and Hart, P., 1999, A seismic-reflection investigation of gas hydrates and sea-floor features of the upper continental slope of the Garden Banks and Green Canyon regions, northern Gulf of Mexico: Report for cruise G1-990GM (99002): U.S. Geological Survey Open-File Report 99-570, 18 p.

Deregowski, S.M., 1986, What is DMO?: First Break, v. 4, p. 7–24.

Deregowski, S., and Rocca, F., 1981, Geometrical optics and wave theory for constant-offset sections in layered media: Geophysical Prospecting, v. 29, p. 374–387.

Dillon, W.P., Booth, J.S., Paul, C.K., Felhaber, K., Hutchinson, D.R., and Swift, B.A., 1991, Mapping sub-seafloor reservoirs of greenhouse gas: Methane hydrate, *in* Kumar, M., and Maul, G.A., eds., Proceedings of International Symposiums on Marine Positioning: Washington, D.C., Marine Geodesy Committee, Marine Technology Society, p. 545–554.

Dillon, W.P., Lee, M.W., Fehlhaber, K., and Coleman, D.F., 1993, Gas hydrates on the Atlantic continental margin of the United States—Controls on concentration, *in* Howell, D.G., ed., The Future of Energy Gases: U.S. Geological Survey Professional Paper 1579, p. 313–330.

Gray, W.C., 1979, Variable norm deconvolution: Palo Alto, Calif., Stanford University Ph.D. thesis, 101 p.

Grow, J.A., Lee, M.W., Miller, J.J, Agena, W.F., Hampson, J.C., Foster, D.S., and Woellner, R.A., 1986, Multichannel seismic-reflection survey of KOA and OAK craters, *in* Folger, D.W., ed., Sea-Floor Observations and Subbottom Seismic Characteristics of OAK and KOA Craters, Eniwetok Atoll, Marshall Islands: U.S. Geological Survey Bulletin 1678, p. D1–D46.

Kvenvolden, K.A., 1993, A primer of gas hydrates, *in* Howell, D.G., ed., The Future of Energy Gases: U.S. Geological Survey Professional Paper 1579, p. 555–561.

Lee, M.W., 1999, Processing of single channel air and water gun data for imaging an impact structure at the Chesapeake Bay: U.S. Geological Survey Bulletin 2169, 7 p. [*available online at* http://greenwood.cr.usgs.gov/pub/bulletins/b2169/index.html].

Paul, C.K., Ussler, W., III, and Dillon, W.P., 1991, Is the extent of glaciation limited by marine gas-hydrates?: Geophysical Research Letters, v. 18, p. 432–434.

Poag, C.W., Hutchinson, D.R., Colman, S.M., and Lee, M.W., 1999, Seismic expression of the Chesapeake Bay impact crater: Structural and morphologic refinements based on new seismic data, *in* Dressler, Burkhard, and Sharpton, V.L., eds., Impact Cratering and Planetary Evolution II: Boulder, Colo., Geological Society of America Special Paper 339, p. 149–164.

Wiggins, R.A., 1977, Minimum entropy deconvolution: Proceedings of the International Symposium on Computer-Aided Seismic Analysis and Discrimination, June 9–10, Falmouth, Mass., IEEE Computer Society, p. 7–14.

Yilmaz, Ozdogan, 1987, Seismic data processing: Society of Exploration Geophysicists—Investigations in Geophysics, v. 2, 526 p.

Appendix

The arrival times of source/receiver ghosts can be calculated easily assuming a flat water-bottom topology and a straight ray path.

Let V be the water velocity, S be the source depth, R be the receiver depth, H be the water depth, and G be the offset. By defining $H_1 = H–S$ and $H_2 = H–R$, the arrival time can be written as follows:

(a) Source and receiver ghost arrival time (T_{rs}):

$$T_{rs} = (2\sqrt{S^2 + X_1^2} + 2\sqrt{R^2 + X_2^2} + \sqrt{H_1^2 + X_3^2} + \sqrt{H_2^2 + X_4^2})/V \qquad \text{(A1)}$$

where

$$X_1 = \frac{SG}{2S + 2R + H_1 + H_2},$$

$$X_2 = \frac{RG}{2S + 2R + H_1 + H_2},$$

$$X_3 = \frac{H_1 G}{2S + 2R + H_1 + H_2}, \text{ and} \qquad \text{(A2)}$$

$$X_4 = \frac{H_2 G}{2S + 2R + H_1 + H_2}.$$

(b) Primary reflected arrival time (T_p):
T_p = equation A1 with $S = 0$ and $R = 0$ in X's in equation A2.

(c) Source ghost arrival time (T_s):
T_s = equation A1 with $R = 0$ in X's in equation A2.

(d) Receiver ghost arrival time (T_r):
T_r = equation A1 with $S = 0$ in X's in equation A2.

Manuscript approved for publication December 4, 2000
Published in the Central Region, Denver, Colorado
Graphics by the authors
Editing, page layout, and photocomposition by
Richard W. Scott, Jr.